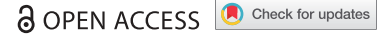


REPORT



## DYRK1A regulates the recruitment of 53BP1 to the sites of DNA damage in part through interaction with RNF169

Vijay R. Menon<sup>a\*†</sup>, Varsha Ananthapadmanabhan<sup>a\*</sup>, Selene Swanson<sup>b</sup>, Siddharth Saini<sup>a</sup>, Fatmata Sesay<sup>a</sup>, Vasily Yakovlev<sup>c</sup>, Laurence Florens<sup>b</sup>, James A. DeCaprio<sup>d</sup>, Michael P. Washburn<sup>e</sup>, Mikhail Dozmorov<sup>f</sup>, and Larisa Litovchick<sup>a</sup>

<sup>a</sup>Division of Hematology, Oncology, and Palliative Care, Department of Internal Medicine, Virginia Commonwealth University, Richmond, VA, USA; <sup>b</sup>Stowers Institute for Medical Research, Kansas City, MO, USA; <sup>c</sup>Department of Radiation Oncology, Virginia Commonwealth University, Richmond, VA, USA; <sup>d</sup>Department of Medical Oncology, Dana-Farber Cancer Institute and Department of Medicine, Brigham and Women's Hospital, Harvard Medical School, Boston, MA, USA; <sup>e</sup>Stowers and Department of Pathology and Laboratory Medicine, The University of Kansas Medical Center, Kansas City, KS, USA; <sup>f</sup>Department of Biostatistics and Massey Cancer Center, Virginia Commonwealth University, Richmond, VA, USA

### ABSTRACT

Human Dual-specificity tyrosine (Y) Regulated Kinase 1A (DYRK1A) is encoded by a dosage dependent gene whereby either trisomy or haploinsufficiency result in developmental abnormalities. However, the function and regulation of this important protein kinase are not fully understood. Here, we report proteomic analysis of DYRK1A in human cells that revealed a novel role of DYRK1A in DNA double-strand breaks (DSBs) repair, mediated in part by its interaction with the ubiquitin-binding protein RNF169 that accumulates at the DSB sites and promotes homologous recombination repair (HRR) by displacing 53BP1, a key mediator of non-homologous end joining (NHEJ). We found that overexpression of active, but not the kinase inactive DYRK1A in U-2 OS cells inhibits accumulation of 53BP1 at the DSB sites in the RNF169-dependent manner. DYRK1A phosphorylates RNF169 at two sites that influence its ability to displace 53BP1 from the DSBs. Although DYRK1A is not required for the recruitment of RNF169 to the DSB sites and 53BP1 displacement, inhibition of DYRK1A or mutation of the DYRK1A phosphorylation sites in RNF169 decreases its ability to block accumulation of 53BP1 at the DSB sites. Interestingly, CRISPR-Cas9 knockout of DYRK1A in human and mouse cells also diminished the 53BP1 DSB recruitment in a manner that did not require RNF169, suggesting that dosage of DYRK1A can influence the DNA repair processes through both RNF169-dependent and independent mechanisms. Human U-2 OS cells devoid of DYRK1A display an increased HRR efficiency and resistance to DNA damage, therefore our findings implicate DYRK1A in the DNA repair processes.

### KEYWORDS

Proteomic analysis; phosphorylation; DNA double strand break repair; DYRK1A knockout cells; DYRK1A-interacting proteins

## Introduction

Gene dosage imbalance that involves regulatory genes, such as *DYRK1A*, could have dramatic consequences for the individual cells, tissues, organs or entire organisms [1,2]. In case of *DYRK1A*, both gain and loss of one allele result in developmental abnormalities. Trisomy of a critical region on human chromosome 21 where the *DYRK1A* gene is located results in Down syndrome (DS) [3,4]. Loss or intragenic deletion affecting one copy of the *DYRK1A* gene has also been recently recognized as a syndrome characterized by microcephaly and severe mental retardation [5,6]. The requirement of the proper *DYRK1A* gene dosage


for neurological development is conserved in evolution, as evident from genetic studies of its *Drosophila* orthologue *minibrain* (*mnbr*) [7,8]. Furthermore, mouse models of *Dyrk1a* trisomy recapitulate some of the DS phenotypes [9–11]. Homozygous deletion of *Dyrk1a* causes early embryonic lethality whereas *Dyrk1a*<sup>+/-</sup> animals have reduced brain size as well as specific neurological and behavioral defects [12,13]. In order to explain these phenotypes, it is important to understand the function and regulation of DYRK1A.

DYRK1A belongs to the CMGC group of protein kinases that also includes cyclin-dependent kinases (CDKs), mitogen activated protein kinases

**CONTACT** Larisa Litovchick ✉ [larisa.litovchick@vcuhealth.org](mailto:larisa.litovchick@vcuhealth.org)

\*These authors contributed equally to this work.

†Present address: Department of Cell, Developmental and Regenerative Biology, Icahn School of Medicine at Mount Sinai, 1425 Madison Avenue, New York, NY 10029  
This article has been republished with minor changes. These changes do not impact the academic content of the article.

 Supplemental data for this article can be accessed [here](#).

© 2019 The Author(s). Published by Informa UK Limited, trading as Taylor & Francis Group.

This is an Open Access article distributed under the terms of the Creative Commons Attribution-NonCommercial-NoDerivatives License (<http://creativecommons.org/licenses/by-nc-nd/4.0/>), which permits non-commercial re-use, distribution, and reproduction in any medium, provided the original work is properly cited, and is not altered, transformed, or built upon in any way.

(MAPKs), glycogen synthase kinases (GSKs), and CDK-like kinases (CLKs) [14,15]. Functionally, DYRK1A is a dual-specificity protein kinase that regulates several protein substrates, some of which are involved in control of the cell cycle and transcription including cyclin D1, p27, RNA polymerase II and LIN52 subunit of the DREAM repressor complex [16–21]. DYRK1A preferentially phosphorylates protein substrates that match the consensus R-X(XX)-S-P where X is any amino acid [22,23] although some substrates such as cyclin D1 contain alternative phosphorylation sites [18,19]. In addition to these potential substrates, DYRK1A interacts with several proteins that may regulate its function or subcellular localization including DCAF7 and 14-3-3 [24–27]. A recent study of the proteomic landscape of the CMGC kinases in HEK293T cells identified 24 cellular proteins specifically interacting with DYRK1A, including DCAF7 [28]. Furthermore, DYRK1A has been shown to interact with several viral proteins including adenovirus E1A and human papilloma virus E6 proteins, and alter their ability to transform host cells [29–32].

Previously, we described a critical role of DYRK1A in the G0/G1 entry in human T98G glioblastoma cells by promoting the assembly of the DREAM transcription repressor complex [20,33,34]. Ectopic expression of DYRK1A suppressed proliferation of several human cell lines such as T98G and U-2 OS, but not HEK293T cells [20], suggesting that DYRK1A function could be influenced in a cell-specific context. Therefore, we sought to characterize DYRK1A interacting proteins in T98G cells, using sensitive MudPIT proteomic analysis approach [20]. Our analysis identified proteins that reproducibly and selectively co-precipitated with DYRK1A, including both previously reported and novel interactions. Here, we describe a novel role of DYRK1A in repair of DNA double-strand breaks (DSB) revealed through its interaction with the ubiquitin-binding protein, RNF169. Upon DNA damage, RNF169 accumulates at the DSBs and promotes homologous recombination repair (HRR) by restraining accumulation of 53BP1, a scaffolding protein associated with non-homologous end joining (NHEJ)-promoting factor, at the DSB sites [35–37]. We found that DYRK1A regulates the

recruitment of 53BP1 to the sites of DNA damage, and therefore the levels of DYRK1A in the cells can affect the choice of DNA repair pathway.

## Results

### *MudPit analysis of DYRK1A-interacting proteins*

DYRK1A plays an essential role in cell cycle control in human T98G cells [20]; therefore, we chose these cells for characterization of DYRK1A-interacting proteins using MudPIT MS/MS proteomic analysis [38]. HA-tagged DYRK1A was expressed in T98G cells (Figure 1(a)), purified using anti-HA affinity matrix and analyzed by MudPIT as previously described [20,34]. Four biological replicates were analyzed for DYRK1A-HA pull-down samples along with 3 GFP-HA (control) samples, resulting in identification of 120 proteins (including DYRK1A) that were detected at least twice in the DYRK1A pull-down samples but not in the GFP controls (Table S1). Previous proteomic analysis of DYRK1A in HEK293 cells identified 24 interacting proteins, 14 of which were also detected in our study (Figure S1(a)) [28]. Furthermore, our analysis detected 51 proteins in 3 out of 4 DYRK1A pull-down repeats and 7 proteins including DYRK1A, DCAF7, FAM117A, FAM117B, LZTS2, RNF169 and TROAP, were identified in all biological replicates. These interacting proteins were also the most enriched in the samples and readily confirmed using reciprocal pull-down assays (Figure 1(b,c) and S1(b,c)). Of note, average enrichment of DCAF7 in the immunoprecipitated samples (as shown by Normalized Spectrum Abundance Factor, or dNSAF [39]), was comparable to that of DYRK1A itself, indicating a potentially stoichiometric interaction (Figure 1(c)). Further bioinformatic analysis of the 51 DYRK1A-binding proteins revealed a complex network of interactions of factors involved in different cellular processes with notable enrichment of the mRNA processing, transcription and DNA damage response functional categories (Figure 1(d, e)). Interestingly, recent proteomic analysis of RNF169 also identified DYRK1A as one of the most enriched interacting proteins [40]. RNF169 is a RING-domain ubiquitin-binding protein that plays a role in the DNA repair signaling by

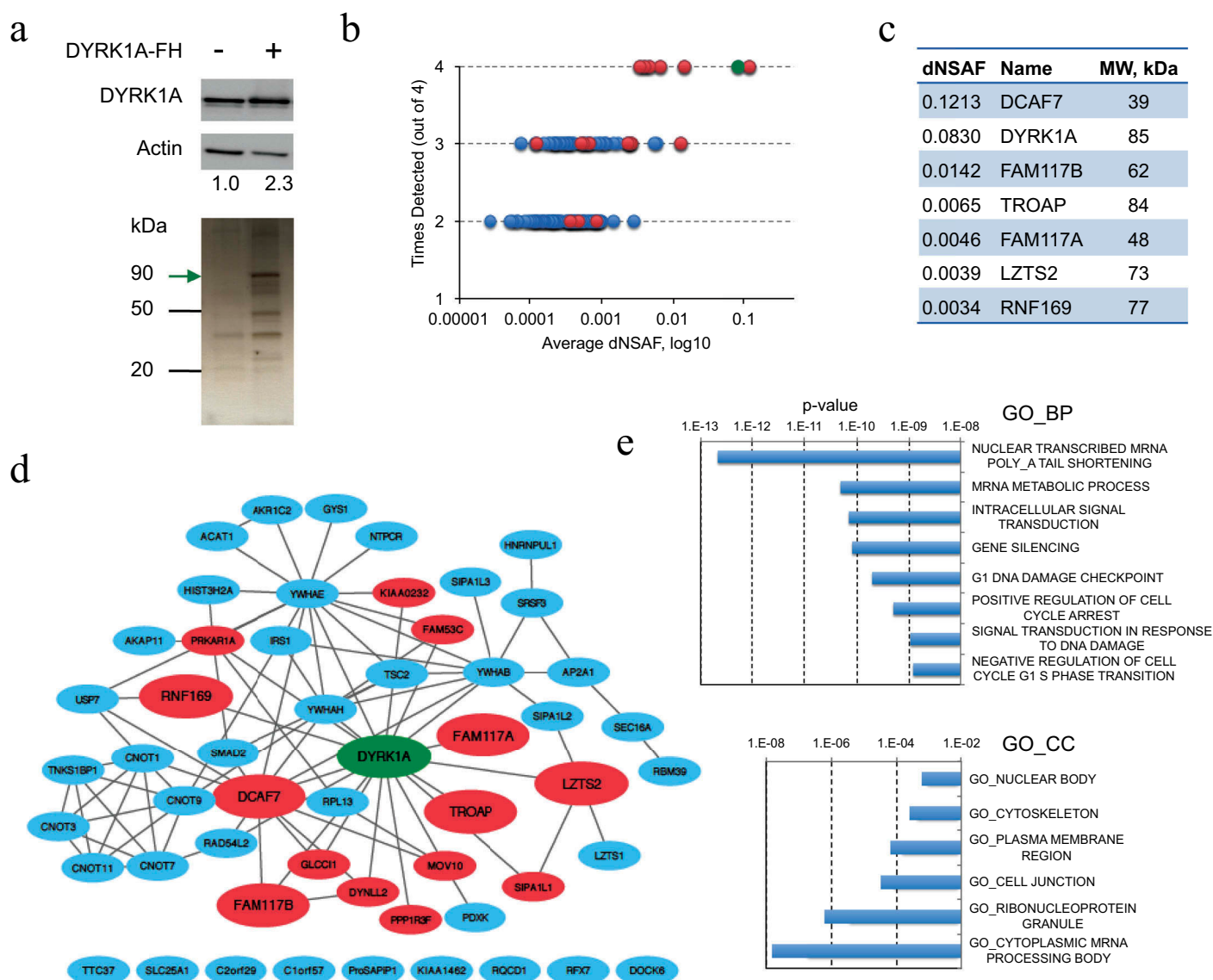


**Figure 1.** Analysis of the DYRK1A-interacting protein network. (a) Purification of DYRK1A for MudPIT proteomic analysis. Top: Western blot showing levels of DYRK1A in T98G cells expressing HA-Flag-tagged DYRK1A (DYRK1A-FH) and DYRK1A band density relative to actin (control). Bottom: representative silver stained gel containing 10% of HA-peptide eluted control or DYRK1A-FH IP samples analyzed by MudPIT. (b) Graph shows relative enrichment (dNSAF) of proteins detected in two, three or all four DYRK1A MudPIT experiments. DYRK1A is shown as green circle whereas red and blue circles correspond to either listed in the BioGrid database [55], or new DYRK1A-binding proteins, respectively. (c) dNSAF (corresponds to relative enrichment) and molecular weight (MW) of seven proteins specifically detected in four DYRK1A-FH MudPIT replicate experiments. (d) Hierarchical network of interactions (CytoScape) involving DYRK1A-binding proteins identified in this study, constructed using MetaScape analysis tool [42]. Colors, same as in B. Larger nodes correspond to proteins detected in all four replicates. Unconnected nodes are not known to interact with other factors. (e) Molecular Signature Database (MSigDB) annotation of the genes encoding DYRK1A-interacting proteins reveals significantly enriched functional gene ontology (GO) categories. Proteins detected in at least 3 DYRK1A MudPIT repeats were analyzed using Molecular Signature Database annotation tool to compute overlaps with GO Biological Process (GO\_BP) and GO Cellular Component (GO\_CC) gene sets [43].

regulating 53BP1, a scaffold protein that plays a key role in the choice of the double strand break (DSB) DNA repair by promoting non-homologous end joining (NHEJ) and inhibiting homologous recombination (HR) [35,37,41]. Since the role of DYRK1A in DNA repair processes is not known, we chose to further

characterize the interaction between DYRK1A and RNF169.

#### ***DYRK1A interacts with RNF169 and regulates recruitment of 53BP1 to DSBs***

We confirmed the interaction between RNF169 and DYRK1A at both overexpressed and the endo-

genous levels in a series of immunoprecipitation/Western blot (IP/WB) assays using two different human cell lines, T98G and U-2 OS (Figure 2(a-c)). Furthermore, we found that DYRK1A and RNF169 co-fractionated together in T98G cell extract subjected to a glycerol gradient ultracentrifugation, and estimated the approximate size of the DYRK1A-RNF169 complex as 280 kDa (Figure 2(d)). U-2 OS cells have been previously used to characterize the role of RNF169 in limiting the recruitment of 53BP1 into  $\gamma$ -irradiation-induced foci (IRIF). In the preliminary experiments, we found that U-2 OS cells contained the maximum number of distinct 53BP1 IRIF at 3h after  $\gamma$ -irradiation (5Gy, data not shown). Therefore, we used these conditions to assess the involvement of DYRK1A in the regulation of 53BP1 upon DNA damage in the U-2 OS cell lines stably expressing either wild type or kinase inactive DYRK1A-K188R mutant under control of a doxycycline (dox)-inducible promoter [20,44]. While the interaction between RNF169 and DYRK1A was independent of DYRK1A's kinase activity (Figure 2(e)), induced expression of active, but not the kinase-inactive DYRK1A in U-2 OS cells resulted in significantly decreased number of cells displaying more than ten 53BP1 IRIF compared to the un-induced control (Figure 2(f,g) and S2(a)). To find out whether this effect required RNF169, we knocked down its expression in DYRK1A-inducible cell lines using siRNA (Figure 2(h)). Indeed, we observed that the recruitment of 53BP1 into IRIF in the active DYRK1A-overexpressing cells was rescued to the control cell levels when RNF169 expression was decreased (Figure 2(i) and S2(b)).

To further investigate the role of DYRK1A kinase activity in regulating RNF169 and 53BP1, we pre-treated U-2 OS parental, or stably expressing HA-RNF169 cells with 10  $\mu$ M of DYRK1A inhibitor harmine for 16h prior to  $\gamma$ -irradiation, and quantified formation of the 53BP1 IRIF. For accurate assessment, we quantified both the percentage of cells containing more than ten IRIF, as well as an average number of IRIF per nucleus, using Image J software [45]. As seen in Figure 3(a,b), pre-treatment of U-2 OS cells with harmine increased the formation of 53BP1 IRIF, supporting the role of DYRK1A in regulation of 53BP1 DSB recruitment at the endogenous levels. In

agreement with previous reports, U-2 OS cells stably expressing HA-RNF169 displayed approximately 50% less cells with more than ten 53BP1 foci, and had fewer IRIF per nucleus (Figure 3(a,b), compare gray bars). Treatment of these cells with harmine resulted in a significant increase of the 53BP1 foci formation although it was not rescued to the control levels (Figure 3(a,b), red bars and graph on the right Y-axis). Interestingly, HA-RNF169 foci formation was decreased by approximately 30% in harmine-treated cells compared to controls (Figure 3(c), compare green bars), which could explain an increased formation of 53BP1 IRIF upon harmine treatment. As in case of the kinase-inactive DYRK1A protein (Figure 2(e)), the binding between RNF169 and DYRK1A was unaffected by harmine inhibition (Figure 3(d)). Together, these results show that RNF169 and DYRK1A interact at the endogenous levels in human cells, and that DYRK1A facilitates the RNF169's ability to limit the accumulation of 53BP1 at the DSB sites.

#### **DYRK1A phosphorylates functionally important Ser368 and Ser403 residues in RNF169**

The RNF169 protein sequence contains two predicted DYRK1A consensus sites R-X(XX)-S-P [23]. These sites, S386 and S403, are located within a highly conserved amino acid region in RNF169 that has no known function (Figure S3(a)). Importantly, *in vivo* phosphorylation of these sites in human RNF169 was detected in several high-throughput proteomic studies reported in the PhosphoSitePlus database [46]. To determine whether DYRK1A can phosphorylate S368 or S403 in RNF169, we performed *in vitro* kinase assays using HA-tagged RNF169, S386A- or S403A- or S368A/S403A-RNF169 transiently expressed in HEK293T cells and immunoprecipitated, as substrates for recombinant purified DYRK1A. To diminish any co-precipitating kinase activity, HA-RNF169 immunoprecipitates were heat-inactivated at 65°C for 10 min prior to incubation with DYRK1A. As predicted, we observed that RNF169 was phosphorylated by DYRK1A, and that each of the S368A or S403A mutations decreased the RNF169 phosphorylation while the mutation of both sites further reduced the RNF169 phosphorylation (Figure S3(b,c)). It should be noted that some residual phosphorylation (approximately 10% of the wild-type RNF169 levels) could be detected in the S368A/S403A (RNF169-AA)



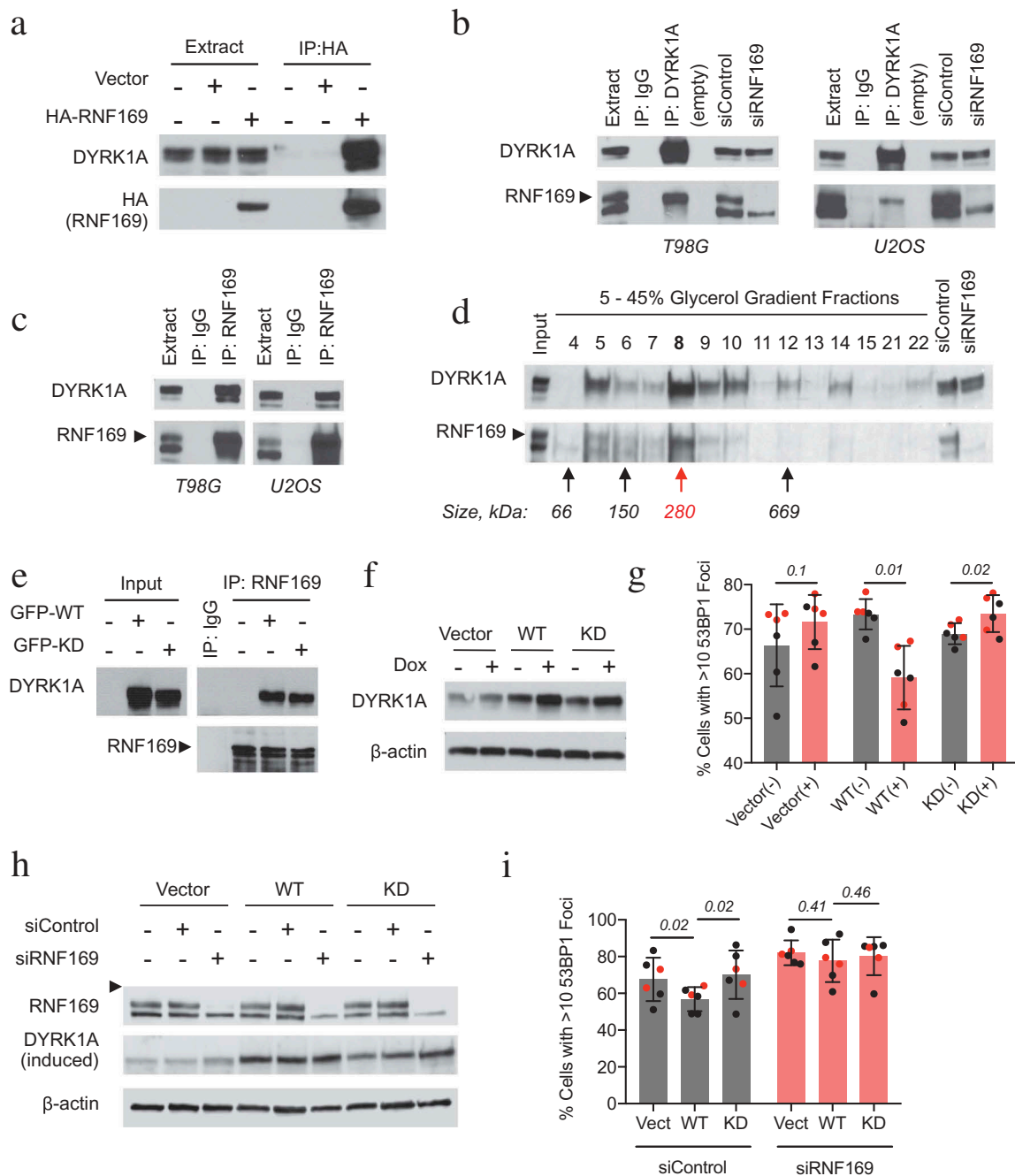


**Figure 2.** DYRK1A and RNF169 interact at the endogenous level and regulate 53BP1. (a) IP/WB assay shows binding between transiently expressed HA-tagged RNF169 and endogenous DYRK1A in T98G cells. (b, c) IP/WB analyzes of the interaction between the endogenous RNF169 and DYRK1A in T98G and U-2 OS cells. RNF169-depleted cell extract (siRNF169) is included to identify the RNF169-specific protein band. IgG, negative control. (d) WB of the U-2 OS cell extract separated by 5–45% glycerol gradient ultracentrifugation shows co-fractionation of RNF169 and DYRK1A. Black arrows indicate the positions of the molecular weight markers. Red arrow indicates estimated size of the DYRK1A-RNF169 complex. (e) IP/WB assay shows interaction between the wild-type and the kinase-inactive DYRK1A (Y321F) and the endogenous RNF169 in U-2 OS cells. (f) WB shows the DYRK1A levels before and after doxycycline (Dox) treatment of the inducible U-2 OS cell lines. Actin is shown as loading control. (g) Induced expression of active but not kinase-inactive (KD) DYRK1A (K188R) inhibits the 53BP1 IRIF formation. Inducible U-2 OS cell lines were pre-incubated with or without Dox for 12h, treated with radiation (5 Gy) and processed for 53BP1 staining after 3h. Graph shows quantification of cells with 53BP1 foci in cell lines with (+) or without (-) Dox induction of 3 biological replicate experiments by two independent observers (here and below shown as black and red dots, p-values calculated using Student's two-tailed t-test). (h, i) Knockdown of RNF169 rescues DYRK1A-mediated inhibition of 53BP1 foci formation. Inducible U-2 OS cell lines were transfected with non-targeting (siControl) or RNF169-specific siRNA and treated with doxycycline to induce expression of DYRK1A. WB in panel H shows expression of proteins of interest. Panel I shows quantification of the 53BP1 foci in cells collected 3h after irradiation.

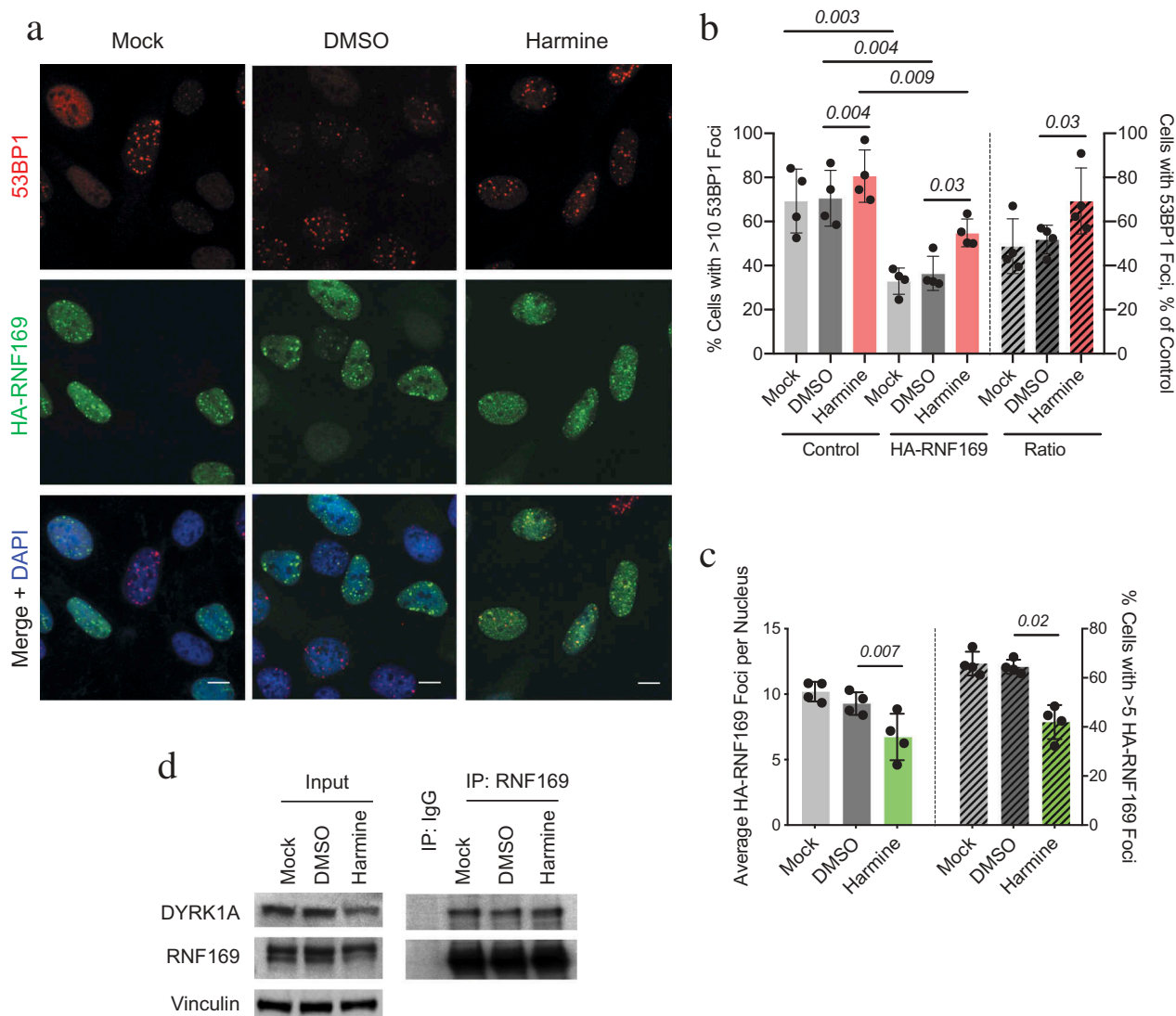


**Figure 3.** Inhibition of DYRK1A increases 53BP1 recruitment to IRIF. (a) Representative images of HA-RNF169 and 53BP1 irradiation-induced foci in U-2 OS cells stably expressing HA-RNF169 that were either untreated (Mock), or pre-treated with 10  $\mu$ M harmine or DMSO (vehicle) for 16h before irradiation (5 Gy) and processed for staining after 3h. (b, c) Graphs show quantification of the 53BP1 (b) or HA-RNF169 (c) IRIF from 4 biological replicate experiments. (d) IP/WB shows that DYRK1A-RNF169 interaction is unaffected by harmine treatment.

mutant. This could be due to a presence of additional, non-canonical DYRK1A phosphorylation site(s) in RNF169, or because of the contaminating kinase activity in the recombinant DYRK1A preparation.

To further characterize the functional significance of DYRK1A phosphorylation sites in RNF169, we analyzed localization of 53BP1 and RNF169 after  $\gamma$ -irradiation-induced DNA damage in U-2 OS cell lines stably expressing either wild type HA-RNF169, non-phosphorylatable S368A/S340A (RNF169-AA) mutant, or phospho-mimetic S368D/S340D (RNF169-DD) mutant. Interestingly, we observed approximately two-fold higher number of cells with more than ten 53BP1 foci in either RNF169-AA- or

RNF169-DD-expressing cells compared to the wild type HA-RNF169 cell line (Figure 4(a,b)). The number of 53BP1 foci per nucleus was also modestly but significantly increased in the cells expressing mutant RNF169 alleles compared to the wild-type expressing cells, indicating that phospho-site mutant RNF169 proteins inhibit accumulation of 53BP1 at DSB sites to a significantly lesser extent than the wild type RNF169 (Figure 4(a,b)). This result is consistent with the effect of harmine, supporting the contribution of DYRK1A to the RNF169-mediated inhibition of 53BP1 accumulation at the DSB sites.

Next, we investigated the recruitment of the HA-RNF169-AA and DD mutants to DSB sites in  $\gamma$ -

irradiated U-2 OS cell lines. Interestingly, we observed a slight but significant decrease in the number of HA-positive foci in the cells expressing the mutant proteins as compared to the wild type RNF169 (Figure 4(c)). We also noted that foci formed by the mutant HA-RNF169 proteins appeared to be larger in size than in case of the wild type protein. Indeed, measurement of the foci size using Image J software confirmed a significant increase of the mean size of the RNF169-AA and DD foci compared to the wild type control (Figure 4(d)), although the expression levels of these RNF169 alleles were similar (Figure S3(d)). Since the phenotypes of RNF169-DD mutant were very similar to that of RNF169-AA, it is possible that S368D/S403D mutation does not accurately represent a constitutively phosphorylated state of the protein but instead disrupts the same function as in case of the S368A/S403A mutation. Therefore, we tested whether any known functions of RNF169 were impacted by mutation of the DYRK1A phosphorylation sites. Previous studies found that the recruitment of RNF169 at the DSB sites and displacement of 53BP1 require ubiquitin-binding MIU domain of RNF169 that recognizes RNF168-polyubiquitylated chromatin at the site of damage [35,37,47]. Both the RNF169-AA and RNF169-DD mutants were able to bind polyubiquitin chains similar to the wild type RNF169, further supporting our conclusion that S368 and S403 sites do not play a significant role in RNF169's accumulation at the DSB sites (Figure S3(e)). Furthermore, mutations of these sites did not affect the interaction with ubiquitin-specific protease USP7 that has been shown to be important for RNF169 function in DNA repair [40] (Figure 4(e)). However, we found that both mutants showed a dramatically reduced binding to DYRK1A, both in the intact cells and after treatment with  $\gamma$ -irradiation (Figure 4(e,f)).

Therefore, our data presented above support the conclusion that DYRK1A binding and phosphorylation of RNF169 increases its ability to limit the recruitment of 53BP1 at the DSB sites after  $\gamma$ -irradiation.

### **Loss of DYRK1A results in a decreased DSB recruitment of RNF169 and 53BP1**

To further investigate the effects of DYRK1A loss on 53BP1 and RNF169 function, we generated U-2 OS cell lines harboring frame-shift mutations in *DYRK1A*

gene by CRISPR-Cas9 gene editing approach [48]. Of note, the Cell Line Encyclopedia data show a partial loss of chromosome 21 harboring the *DYRK1A* gene in U-2 OS [49]. Using DNA FISH, we confirmed presence of a single copy of the *DYRK1A* gene in U-2 OS cells (Figure S4(a)). To obtain DYRK1A knockout (KO) cells, we transiently expressed Cas9 endonuclease and DYRK1A-specific guiding RNA in U-2 OS cells, isolated individual single-cell clones and screened them for loss of DYRK1A protein expression using WB. Two independent U-2 OS DYRK1A-KO clones were expanded and further validated by WB and genomic DNA sequencing (Figure 5(a) and S4(b, c)). Furthermore, we confirmed a significant loss of DYRK1A kinase activity in the U-2 OS DYRK1A-KO cell lines using a whole cell extract *in vitro* kinase assay with purified LIN52 as substrate, and a phosphospecific antibody against LIN52-S28 site for detection (Figure S4(d)). Of note, both transient siRNA knockdown or stable shRNA knockdown of DYRK1A resulted in significantly higher residual LIN52 kinase activity detected using this assay (data not shown); therefore, we used the DYRK1A-KO cells to further characterize the role of DYRK1A in the DNA DSB response.

First, we compared the recruitment of RNF169 into the IRIF in the control and the DYRK1A-KO U-2 OS cells. Similar to U-2 OS cells treated with DYRK1A inhibitor harmine (Figure 3(e)), HA-RNF169 displayed a modest but significant decrease in the recruitment to DSBs when transiently expressed in  $\gamma$ -irradiated U-2 OS DYRK1A-KO cell lines compared to controls (Figure 5(b)). We also confirmed this result by using transiently expressed GFP-RNF169 (Figure 5(c)). However, unlike harmine-treated cells (Figure 3(c)), DYRK1A-KO cell lines showed significantly reduced 53BP1 IRIF formation at 3h post  $\gamma$ -irradiation when compared to control cell lines (Figure 5(e,f)). Accumulation of 53BP1 at the DSB sites in the DYRK1A-KO cell lines did not increase at 6h post  $\gamma$ -irradiation, and both DYRK1A-KO cell lines continued to display a significantly decreased 53BP1 IRIF recruitment compared to controls (Figure 5(e,f)).

Since U-2 OS cells could have intrinsically reduced DYRK1A expression resulting from loss of one copy of the *DYRK1A* gene, we further validated our findings described above using mouse NIH-3T3 fibroblasts in which *Dyrk1a* was similarly

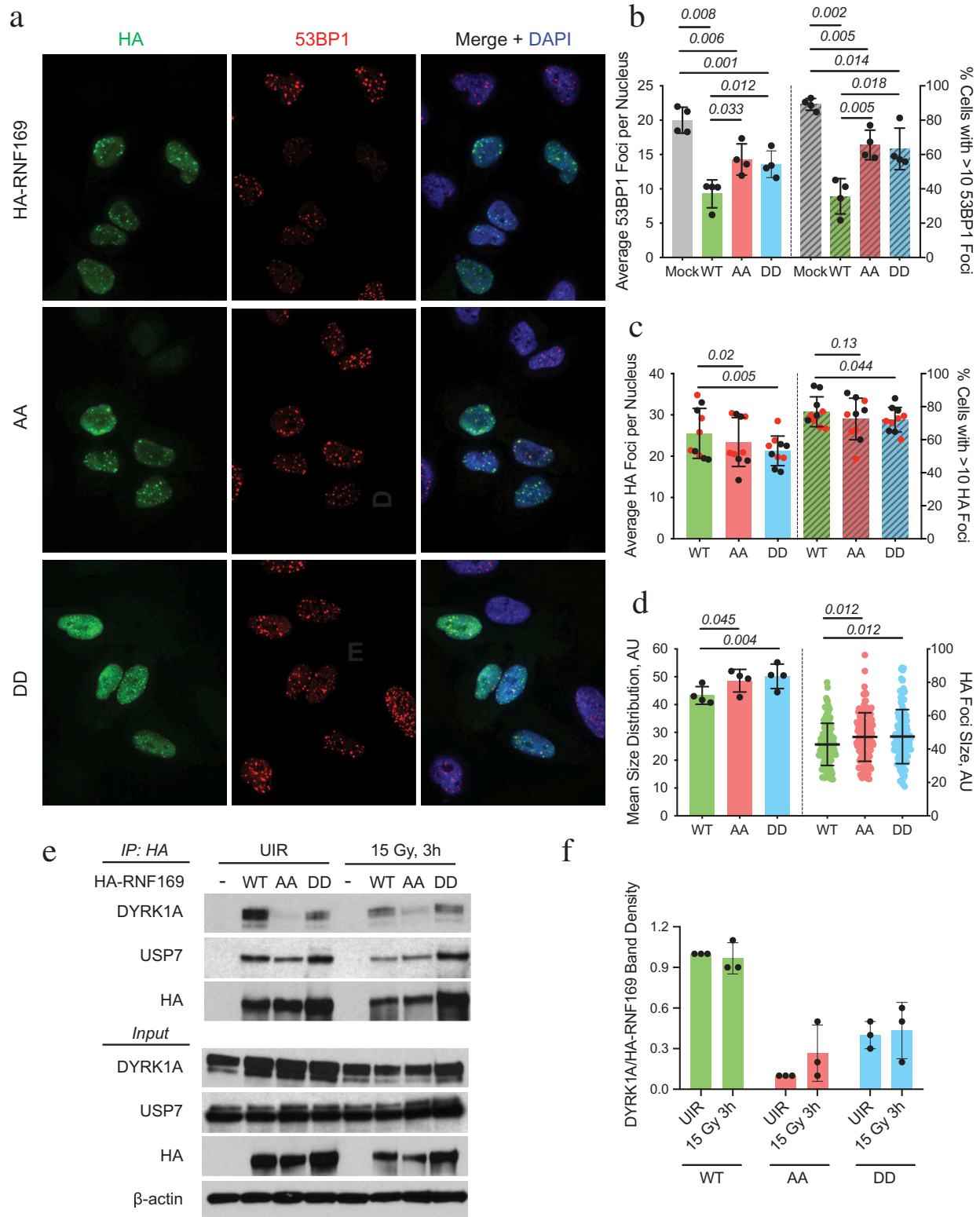


**Figure 4.** The functional significance of S368 and S403 residues in RNF169. (a) Representative images of the HA-RNF169 (green) and 53BP1 (red) foci 3h after  $\gamma$ -radiation (5 Gy). U-2 OS stable cell lines expressing HA-RNF169 (WT), or the S368A/S403A (AA), or S368D/S403D (DD) mutants were stained using anti-HA and 53BP1 antibodies, and DAPI. (b) Graph shows quantification of the 53BP1 IRIF from 4 biological replicate experiments shown in panel A. All cells were scored in the control U-2 OS cells (Mock, shown as reference) whereas only HA-positive cells were scored in the HA-RNF169, AA-RNF169 or DD-RNF169 expressing cell lines. (c) Graph shows quantification of HA-RNF169 IRIF from 4 experiments in A scored by two independent observers (red and black dots). (d) Quantification (average foci sizes, left Y-axis and size distribution, right Y-axis) of HA-RNF169 foci sizes measured in 4 biological replicate experiments. (e) Co-immunoprecipitation assay shows that disruption of the DYRK1A phosphorylation sites in RNF169 affects its interaction with DYRK1A but not USP7. (f) Quantification of HA-RNF169 band density in the IP samples relative to DYRK1A from 3 independent experiments shown in panel E. Relative abundance of DYRK1A to wild-type HA-RNF169 in untreated cells was taken as 1. Differences between the wild-type and the mutant RNF169 alleles were significant under all conditions ( $p < 0.01$ ) while the differences between the AA and DD mutants, or between the control and irradiates samples were not significant.



knocked out using CRISPR-Cas9 approach (Figures S5(a,b)). In case of NIH-3T3 cells, accumulation of 53BP1 foci reaches its peak at 1h post  $\gamma$ -irradiation (3Gy), and then starts to decrease at 3h (data not shown). Using these experimental conditions, we again observed a decreased 53BP1 IRIF formation in two independent, clonal NIH-3T3 Dyrk1a-KO cell lines compared to control cells (Figure S5(c)). Indeed, while majority of the control and Dyrk1a-KO NIH-3T3 cells contained more than ten 53BP1 foci at 1h post  $\gamma$ -irradiation, the average number of 53BP1 IRIF per nucleus was significantly lower in the Dyrk1a-KO cells compared to control (Figure S5(c)). At 3h post  $\gamma$ -irradiation, the number of 53BP1 foci per nucleus decreased by approximately 50% in both the control and Dyrk1a-KO cell lines, indicative of a similar rate of resolving the lesions and removal of 53BP1 foci in these cells lines.

To further confirm that the phenotype of the DYRK1A-KO U-2 OS cells was specific to a loss of DYRK1A protein and kinase activity, we re-introduced either active DYRK1A, or kinase-inactive K188R-DYRK1A (KD) mutant, into one of our knockout clones. Indeed, we observed that expression of the wild-type DYRK1A, but not the kinase inactive mutant, resulted in a complete rescue of the 53BP1 IRIF defect in these cells (Figures S6(a-c)). Together, these results strongly support the role of DYRK1A in regulation of 53BP1 recruitment to the DNA double strand breaks caused by  $\gamma$ -irradiation.

#### **Depletion of RNF169 does not fully rescue the 53BP1 recruitment defect in DYRK1A-KO cells**

Next, we investigated the impact of DYRK1A loss on the ability of the overexpressed RNF169 to displace 53BP1 from IRIF. Consistent with our findings that RNF169 was able to inhibit 53BP1 IRIF formation when DYRK1A was inhibited by harmine (Figure 3), we observed that overexpression of GFP-RNF169 in the DYRK1A-KO U-2 OS cells also results in inhibition of the 53BP1 recruitment to DSBs (Figure 6(a,b)), the differences between the GFP- and GFP-RNF169-expressing cells were highly significant in all cell lines,  $p < 0.001$ ). Furthermore, recruitment of 53BP1 foci was significantly lower both in the GFP- and GFP-RNF169-transfected DYRK1A-KO cells compared to the corresponding control cell lines

(Figure 6(b)), suggesting that knockout of DYRK1A in U-2 OS cells could impair 53BP1 IRIF formation independent of RNF169.

To determine whether the effect of DYRK1A loss on 53BP1 is mediated by RNF169 or not, we depleted RNF169 in U-2 OS cell lines using siRNA transfection (Figure 6(c)). Interestingly, unlike DYRK1A overexpressing cells (Figure 2(i)), knock-down of RNF169 in DYRK1A-KO U-2 OS cells failed to completely rescue the 53BP1 recruitment to the DSB sites, because the RNF169-depleted DYRK1A-KO cells still showed significantly lower 53BP1 IRIF formation when compared to corresponding control cell lines (Figure 6(d,e)). This result suggests that the 53BP1 recruitment defect in the absence of DYRK1A is not likely due to a more efficient displacement by RNF169. Together, our data support the conclusion that DYRK1A regulates the recruitment of 53BP1 to damaged chromatin in RNF169-dependent as well as independent manner.

To address the mechanism of this 53BP1 recruitment defect, we analyzed the expression of several damage response markers during DNA repair. As shown in Figure S7(a), there was no change in the induction of p53 or  $\gamma$ H2AX in the DYRK1A-KO cells compared to control. Furthermore, loss of DYRK1A in U-2 OS cells did not affect the DNA damage checkpoint, as evident by accumulation of cells in G1 and G2 phases after  $\gamma$ -irradiation (Figure S7(b)). Accumulation of  $\gamma$ H2AX and ubiquitylation of histones at the DNA damage sites also appeared to be unchanged in the DYRK1A-KO cells compared to controls (Figure S7(c)). Since accumulation of both 53BP1 and BRCA1 at the DSB sites requires the activity of RNF168 and RNF8 E3 ubiquitin ligases, we also analyzed the recruitment of BRCA1 in these cells and found it unchanged in the DYRK1A-KO cells (Figure S7(d)). Therefore, we concluded that decreased recruitment of 53BP1 to the damage sites was likely not because of abnormal DNA damage signaling or histone ubiquitylation in the DYRK1A-KO cells.

#### **Loss of DYRK1A promotes the HRR and DNA repair**

Previous studies demonstrated the role of 53BP1 in suppressing the HR-mediated DNA repair by

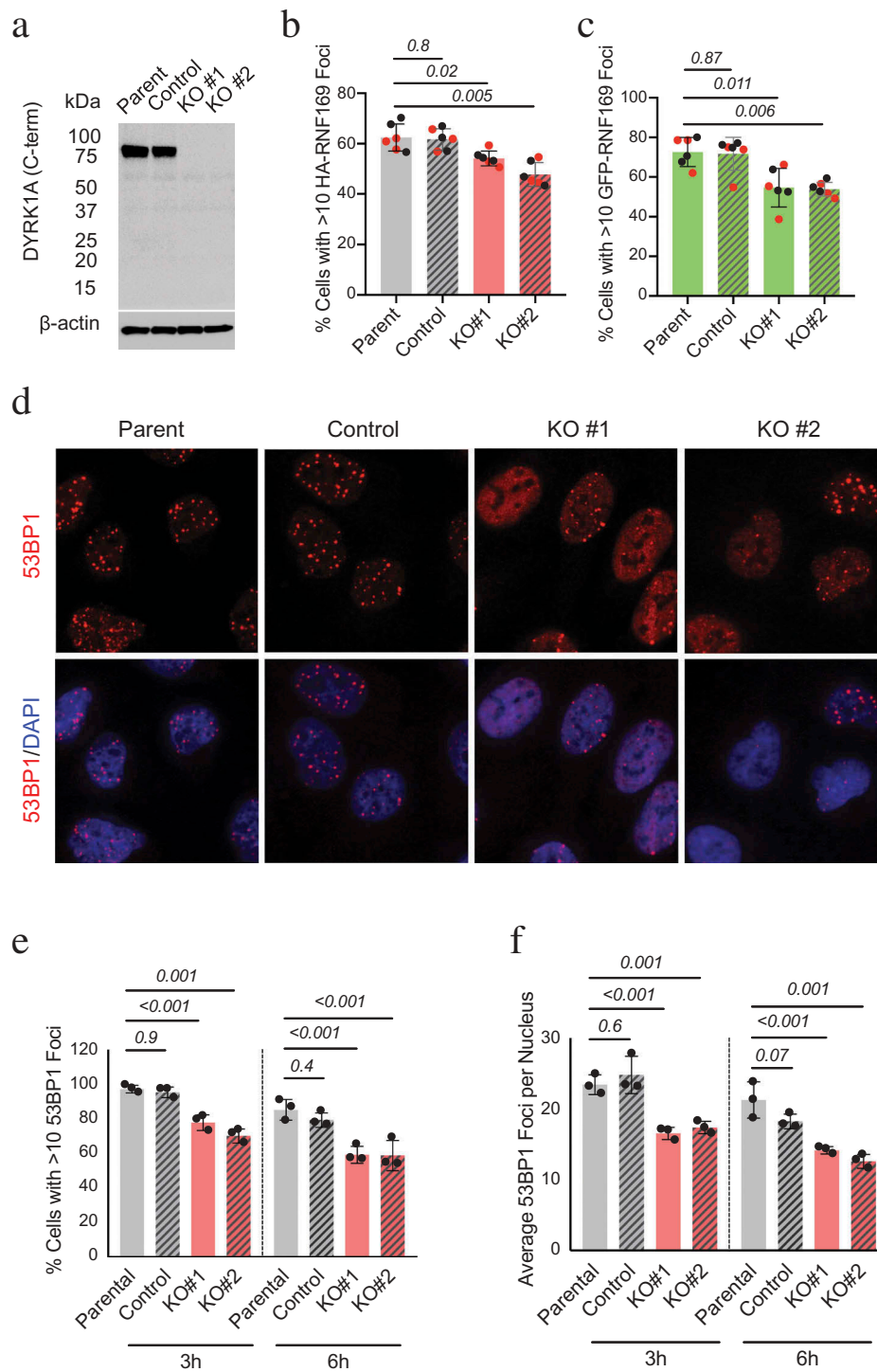


**Figure 5.** DYRK1A-deficient cells have impaired recruitment of RNF169 and 53BP1 to the DSBs. (a) WB confirms absence of the full-length DYRK1A protein expression in two different U-2 OS DYRK1A-KO clones. (b, c) Quantification of HA-RNF169 IRIF in U-2OS cells transiently expressing HA-RNF169 or GFP-RNF169 after 3h post-irradiation (5Gy) of the parental, control (non-targeting sgRNA clone) or DYRK1A-KO U-2 OS cell lines. Red and black dots indicate counts by two independent observers. For statistical analysis, cell lines were compared to the parental U-2 OS cells. (d, e, f) Representative images and quantification of 53BP1 IRIF from the cell lines described above. All cells were processed for staining after 3h and 6h post  $\gamma$ -irradiation (5 Gy). For statistical analysis, each cell line was compared to parental U-2 OS line (gray bars) in three independent experiments.

protecting the DNA ends around the site of damage from resection [50,51]. Since loss of DYRK1A decreased accumulation of 53BP1 at the DSB sites,

we investigated its effect on the DNA repair pathway determination using the control and DYRK1A-KO U-2 OS cell lines stably expressing the direct repeat

(DR) GFP reporter of the HR repair [52]. In this model system, a DSB is generated by cleavage of the non-functional GFP gene fragment by I-SceI restriction nuclease. The break is then repaired either by

NHEJ, resulting in no GFP protein expression, or by HRR, in which case a fluorescent protein is produced (Figure 7(a)). Consistent with reduced recruitment of 53BP1 to DSBs in the DYRK1A-KO cells, we

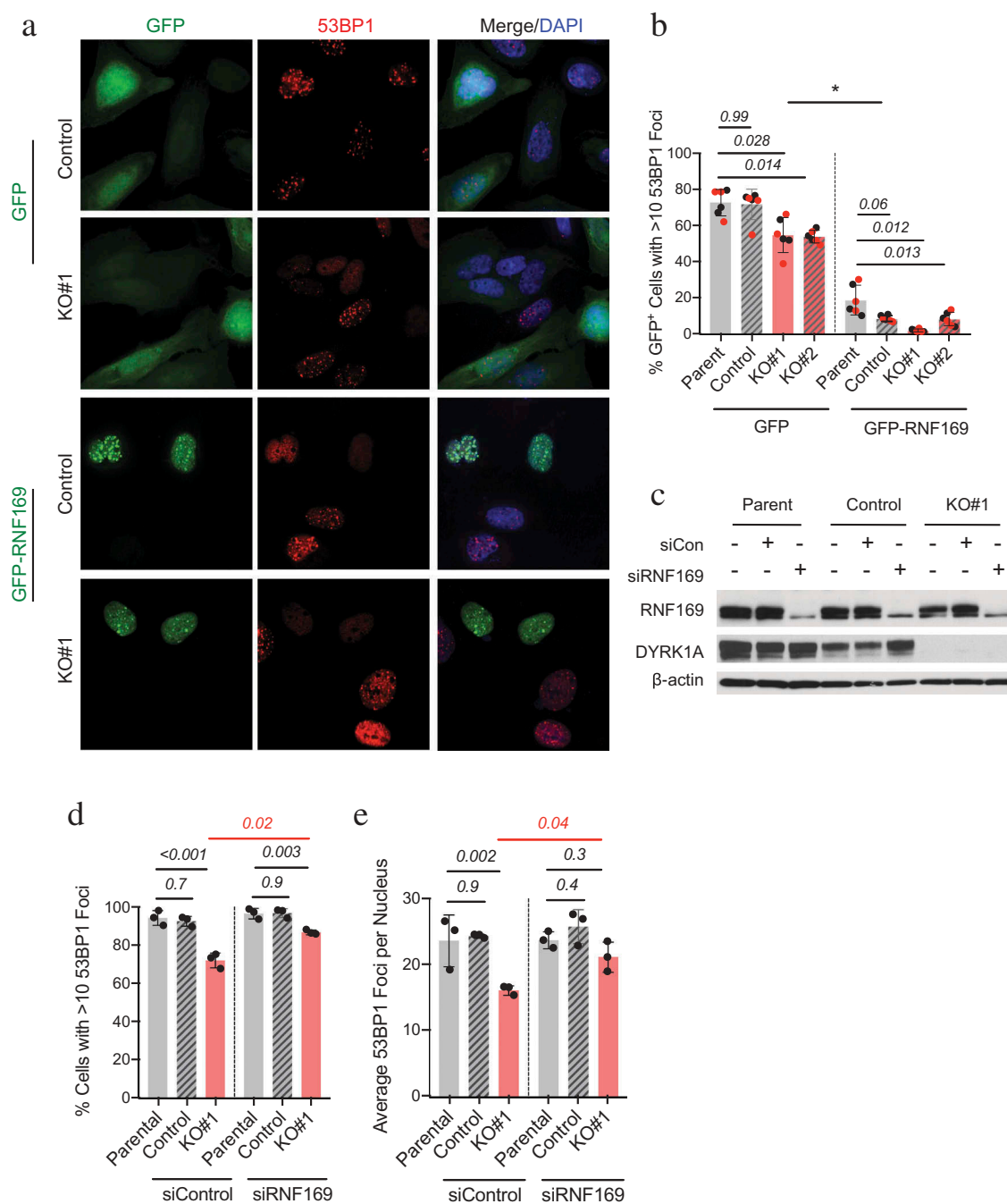


**Figure 6.** Impaired 53BP1 IRIF formation in DYRK1A-KO cells is RNF169 independent. (a, b) Representative images and quantification of GFP-RNF169 (green) and 53BP1 (red) foci 3h after  $\gamma$ -radiation (5 Gy). Indicated U-2 OS cell lines were transiently transfected with GFP or GFP-RNF169 and stained using 53BP1 antibody and DAPI. Data were analyzed using ANOVA with Dunnett's multiple comparisons test (p-values shown). Red and black dots indicate counts by two independent observers. All comparisons between the corresponding GFP-transfected and GFP-RNF169-transfected samples were significant ( $p < 0.01$ ). (c) WB showing the expression levels of RNF169 and DYRK1A in the representative experiment analyzed in panels (d) and (e). (d, e) Quantification of the 53BP1 IRIF in control or DYRK1A-KO U-2 OS cell lines after siRNA knockdown of RNF169.

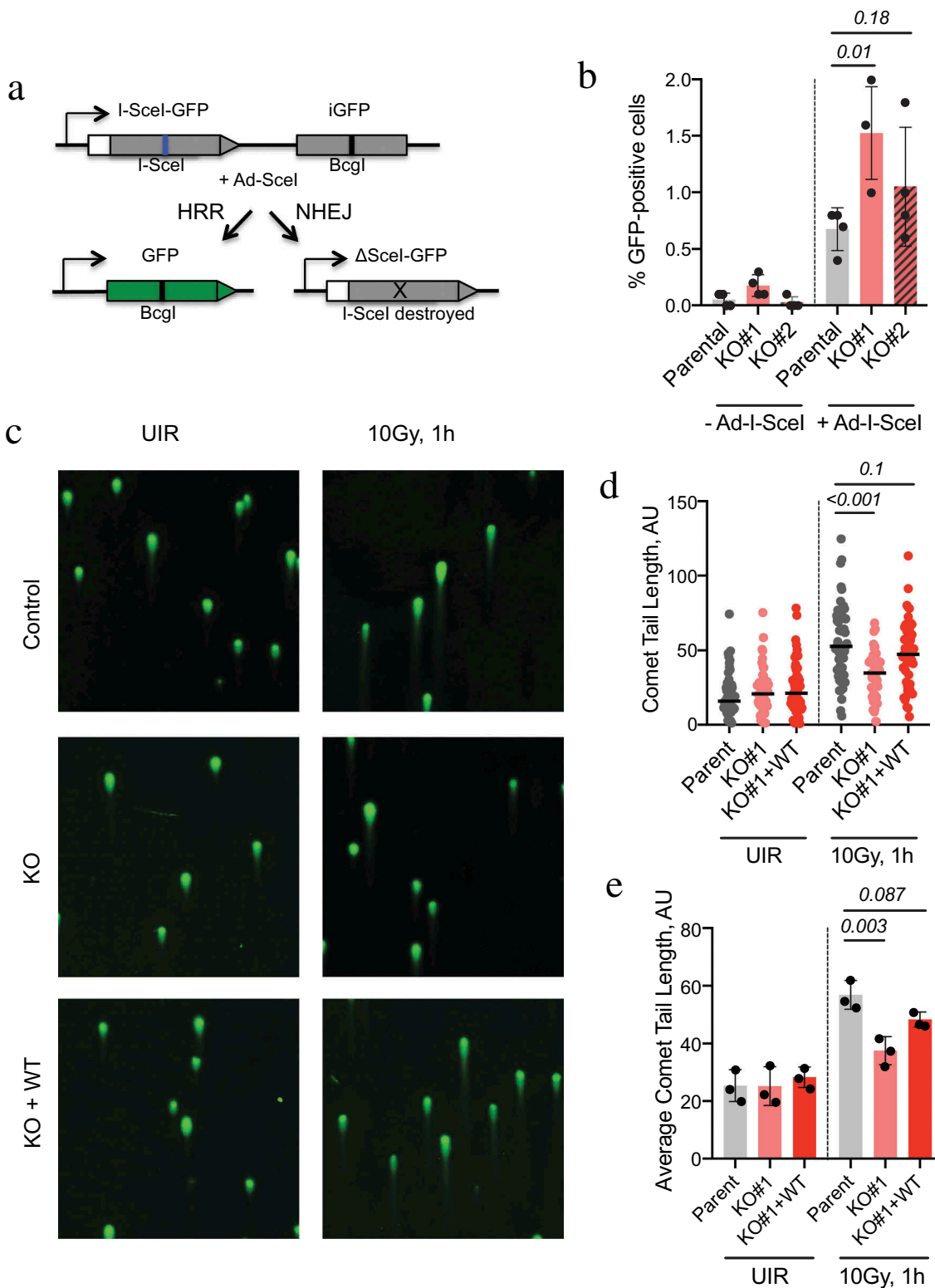


**Figure 7.** Loss of DYRK1A promotes HRR and DNA repair. (a) Schema of the DR-GFP reporter that produces fluorescent protein only after it is cut by I-SceI endonuclease and repaired by HRR [52]. (b) U-2 OS DYRK1A-KO cells display an increased HRR repair efficiency compared to control U-2 OS cells. DR-GFP reporter was stably expressed in the control or DYRK1A-KO cells using transfection followed by antibiotic selection. I-SceI was introduced using adenovirus infection. Graph shows the results of FACS analysis measuring the percentage of GFP-positive cells in the total population in 4 independent I-SceI infection experiments. (c) Neutral comet assay reveals increased DNA integrity in DYRK1A-KO clone #1 compared to control cells or the wild-type DYRK1A-rescued cells (KO+WT) 1h after  $\gamma$ -irradiation (10 Gy). Figure shows representative comet images. (d) Individual points indicate comet tail lengths observed in a representative experiment shown in panel (c). Median comet tail lengths are shown as horizontal lines. (e) E. Quantification of 3 independent experiments shown in panel (c).



observed approximately two fold, significant increase in the percentage of GFP-positive cells after I-SceI expression in one of the DYRK1A-KO clones compared to control U-2 OS cells (Figure 7(b) and S8(a,b)). A similar trend was also observed in the second U-2 OS DYRK1A-KO clone although the differences with the parental control did not reach statistical significance due to high experimental variability.

To determine the effect of DYRK1A loss on the overall efficiency of DNA repair following  $\gamma$ -irradiation, we performed a neutral comet assay using the control U-2 OS cells, DYRK1A-KO and DYRK1A-KO cells with re-expressed wild-type DYRK1A. As shown in Figure 7(c-e), cells lacking DYRK1A displayed significantly shorter comet “tails” containing damaged DNA after 1h post-irradiation (10 Gy) compared to control cells or the DYRK1A-KO cells in which DYRK1A was re-expressed. This result further supports the role of DYRK1A in regulating DNA damage response whereby loss of DYRK1A expression allows more efficient repair of DNA DSB lesions.

## Discussion

*DYRK1A* gene copy number changes have deleterious effects on prenatal and early postnatal brain development and have been linked to neurodegenerative disease and cancer [9,53,54]. Since even subtle changes in DYRK1A levels appear to deregulate its function, it is possible that some effects of *DYRK1A* gene imbalance could be mediated by perturbation of DYRK1A interaction networks. Our data presented here offer an insight into a complexity and functional diversity of the protein-protein interactions that involve this remarkable protein kinase in human cells.

At the time of this manuscript preparation, the BioGrid protein interaction network database listed 80 DYRK1A-interacting proteins, mostly identified by high-throughput affinity-capture mass spectrometric analyzes performed in HEK293T cells [55]. Using sensitive MudPIT proteomic approach [38,56], we identified 120 proteins specifically detected in at least two out of four biological replicate analyzes of DYRK1A

immunoprecipitates from human T98G cells, including 98 proteins not reported to interact with DYRK1A in the BioGrid protein interaction database. Given evidence of the functional significance of DYRK1A in T98G cells [17,20,34], our new data on the DYRK1A protein-protein interaction network in human cells could serve as a resource for the future functional studies of this important protein kinase.

Our analysis identified DCAF7 (also known as WDR68 or HAN11) as most highly enriched in the DYRK1A immunoprecipitates among DYRK1A-binding proteins. Structurally, DCAF7 is a WD40-repeat protein that directly binds to several protein kinases including DYRK1A, and serves as an adaptor to mediate their interactions with other proteins including adenovirus E1A protein [26,27,57]. Furthermore, the DCAF7-mediated interaction of DYRK1A with E1A could alter DYRK1A interacting networks in HEK293T cells because of the presence of this viral protein. Indeed, while fourteen of the DYRK1A-interacting proteins were detected in both T98G and 293T cells (Figure S1(a)), several of the proteins known to interact with E1A including RB1, RBL1, RBL2 and EP300, were not detected in our analysis ([28] and this paper). In addition to its adaptor function, DCAF7 is recruited into the Cul4-DDB1 ubiquitin ligase complex that has been recently shown to regulate stability of DNA ligase I (LIG1), one of the key enzymes in the alternative NHEJ DNA repair [58]. It remains to be determined whether DYRK1A plays a role in the DCAF7-mediated degradation of LIG1 and DNA repair. Importantly, several other proteins that were most enriched in the DYRK1A interactome such as FAM117A and B, LZTS1 and 2, and TROAP, remain to be fully characterized, and their functional connection to DYRK1A is not apparent.

The complexity of the protein-protein interaction network involving DYRK1A could reflect its diverse functions in the context of specific cellular compartments or as part of different protein complexes. Here, we provide functional characterization of the interaction between RNF169 and DYRK1A that revealed the role of DYRK1A in the DNA damage pathway by regulating 53BP1, one of the key response factors to DNA DSB

lesions [41]. The DNA DSBs are repaired in the cell cycle-dependent manner by either homologous recombination repair (HR) or the non-homologous end joining (NHEJ), and the choice of appropriate repair mechanism involves multiple factors that mediate and recognize modifications of the chromatin around the lesion [59]. Ubiquitin ligase RNF168 plays a key role in recruitment of 53BP1 to DSB sites [41,60,61]. RNF168 binds to RNF8-ubiquitylated histones and catalyzes H2A-K15ub modification required for the recruitment of 53BP1 that protects the damaged DNA ends from excision and therefore facilitates the repair by NHEJ [60,62]. RNF169 is a homolog of RNF168 and a relatively new player in the DNA damage response pathway. RNF169 also recognizes H2A-K15ub marks but lacks the E3 ubiquitin ligase activity of its own, therefore its accumulation is thought to limit the recruitment of 53BP1 to DSBs [35,37,47]. The function of RNF169 is best revealed upon its overexpression when it prevents the accumulation of 53BP1 at the DSBs, resulting in increased HR-mediated DNA repair efficiency due to a more efficient resection of the DNA ends [35,37]. However, the mechanism of the RNF169 activity towards 53BP1, as well as the factors that regulate the RNF169 recruitment and dissociation from the DSB sites, are not fully understood.

Our study confirms the role of RNF169 as a negative regulator of 53BP1 accumulation, and supports the role of DYRK1A as an RNF169 kinase that positively regulates its activity through both direct and indirect mechanisms. Previous studies found that a high-affinity ubiquitin-binding MIU domain in RNF169 is required for its ability to inhibit 53BP1 accumulation at the damage sites [35,37,47]. Our study extends this observation by demonstrating that while the binding of RNF169 to the ubiquitylated histones surrounding the DSBs could be necessary, it is not sufficient to prevent the accumulation of 53BP1 at the DSB sites. Indeed, the phosphorylation-deficient RNF169 mutants show reduced ability to displace 53BP1 from the DSBs despite almost normal recruitment to these sites. Interestingly, seven ATM-regulated phosphorylation sites in 53BP1 are required for its interaction with its key effector RIF1 but dispensable for its recruitment to the damage sites [63,64]. It is possible that DYRK1A phosphorylation of RNF169

serves to recruit an additional factor that is essential for displacing 53BP1, or for stabilizing the binding of RNF169 to ubiquitylated chromatin. Constitutive presence of the DYRK1A-RNF169 complex both in the intact cells and after damage, as well as the estimated size of the DYRK1A-RNF169 complex also indicate that other factor(s) is likely present in this complex that could be regulated by DNA damage signaling. Further proteomic studies of the RNF169-DYRK1A complex in the cells before and after DNA damage will help to identify such factor. Of note, our analysis of DYRK1A interactome reported here detected the interaction with USP7, a ubiquitin-specific protease that has been recently shown to bind directly to RNF169 and increase the stability of 53BP1, RNF169 and RNF168 [40,65–67]. Although disruption of the DYRK1A phosphorylation sites in RNF169 did not influence its interaction with USP7, the role of USP7 in the DYRK1A-RNF169 mediated regulation of 53BP1 should be further investigated.

Interestingly, while increased expression of DYRK1A appears to attenuate the displacement of 53BP1 from the DSBs in RNF169-dependent manner, the 53BP1 DSB recruitment defect in the DYRK1A-depleted cells appears to be, at least in part, RNF169-independent. Indeed, DYRK1A-KO cell lines displayed decreased RNF169 IRIF formation, and the 53BP1 recruitment phenotype could not be fully rescued by RNF169 depletion in these cells. Recent studies revealed that in addition to histone H2A-K15ub mark, 53BP1 recognizes and binds to H4K20Me2 mark via its conserved Tudor domain, and this process is regulated by several factors including histone methyltransferases SETD8 and MMSET, as well as Polycomb proteins L3MBTL1 and JMJD2A that occupy these marks in the absence of DNA damage (reviewed in [41]). Furthermore, in S/G2 phases of the cell cycle, BRCA1 plays an active role in removing 53BP1 from chromatin around the damage sites using a complex and not fully understood mechanism that requires CDK activity and CtIP [63,64,68]. It will be interesting to investigate in the future whether changes in these 53BP1-regulating factors are responsible for the phenotypes observed in the DYRK1A-KO cells. Since BRCA1 gene expression could be regulated by DYRK1A through recruitment of the DREAM repressor complex [20,34,69],

the relationship between DYRK1A expression levels and the outcomes of the DNA damaging therapy in cancer should be further investigated. Importantly, loss of 53BP1 can rescue the HR defects associated with inactivation of BRCA1, and could be responsible for the acquired resistance of the BRCA1-mutant tumors to PARP-inhibitor therapy [70]. Therefore, future studies will be needed to establish the exact role of DYRK1A in the context of cellular processes that regulate the recruitment of 53BP1 to the DSBs, and to validate the significance of DYRK1A as a factor that can influence the outcomes of cancer therapy.

## Experimental procedures

### Cell lines

Human osteosarcoma U-2 OS, glioblastoma T98G, HEK293T and mouse NIH-3T3 cells were obtained from ATCC and used from early passage master stocks. Cells were regularly checked for mycoplasma using PCR assay and DAPI staining. T98G cells stably expressing Flag-HA epitope tagged DYRK1A, GFP or DYRK1A-interacting proteins were established using pMSCV retroviral vectors and puromycin selection as described in [20]; this work also describes the doxycycline-inducible U-2 OS cell lines expressing DYRK1A. DYRK1A-KO U-2 OS and NIH-3T3 cells were established using GeneArt CRISPR Nuclease vector with OFP reporter (Life Technologies) harboring human or mouse DYRK1A-specific guide sequences. The control cell line was similarly established using a non-targeting construct provided with the kit. Briefly, cells were transfected with sgRNA-CRISPR plasmids, FACS-sorted for OFP expression and grown as single-cell clones that were screened for DYRK1A expression using immunoblotting. Two different clones lacking DYRK1A expression were expanded and validated using antibodies against different epitopes in DYRK1A as well as genomic sequencing of the nested PCR-amplified fragment surrounding the sgRNA-targeted region. Human DYRK1A-specific guiding sequence for CRISPR-Cas9 genomic mutagenesis: top strand: 5'-tgtaaaggcatatgatcgtg-3' and bottom strand: 5'-cacgatcatatgccttaca-3'. Nested primers for PCR amplification of *DYRK1A* genomic region 400 bp up- and downstream of the Cas9 targeting site: first

PCR set: forward 5'-aagttatctgaagccttctgc-3' and reverse 5'-catggtatgctacatggaaggc-3'; second PCR set: forward 5'-cttaggggtcagggtatctctc-3' and reverse 5'-ccaagatttagactattactac-3'. The second PCR primer set was also used for sequencing of the purified PCR products. Mouse *Dyrk1a*-specific guiding sequence for CRISPR-Cas9 genomic mutagenesis: top strand: 5'-ggacgattccagtcataaga-3', and bottom strand: 5'-tcttatgactggaatcgtcc-3'. Nested primers for PCR amplification of *DYRK1A* genomic region 480 bp up- and downstream of the Cas9 targeting site: first PCR primer set: forward 5'-gaacattgagttcaactttgaggg-3' and reverse 5'-ggcactgactagccagaacc-3'; second PCR primer set: forward 5'-ttgttgggggtccttctg-3' and reverse 5'-caagaagtgagcagcttgctg-3'. To verify clonal origin of established KO cell lines, the amplified genomic regions from the PCR with second primer set were purified, cloned into Promega pGEM<sup>®</sup>-T Easy vector. Multiple DNA clones were sequenced to confirm the presence of mutations and the absence of the wild type sequences.

### Chemicals and treatments

To induce DNA damage, the cells were exposed to gamma irradiation using MDS Nordion Gammacell 40 research irradiator with a <sup>137</sup>Cs source (ON, Canada) to induce DNA damage as described in [37]. Harmine (from Sigma; catalog No. H8646) stock solution was prepared in DMSO, and used for cell treatments at 10 μM final concentrations, respectively.

### RNAi and plasmids

siRNA oligos used in this study were from Ambion/Thermo Fisher Scientific including siRNF169 (Silencer Select, ID: s48512, Cat# 4392420) and Negative Control No.1 siRNA (Silencer Select, Cat# 4390843). siRNA transfections were performed using Lipofectamine RNAiMAX (Invitrogen) according to the manufacturer's instructions. GFP-tagged mouse *Dyrk1a* wild-type and mutant constructs were a kind gift from G. D'Arcangelo [71]. HA-RNF169-pcDNA3 and GFP-RNF169 constructs were a gift from N. Mailand [37]. The phosphosite mutants of RNF169 were generated using the QuikChange II XL site directed mutagenesis kit (Agilent Technologies), and verified by sequencing.

Plasmid transfections were performed using either TransIT-2020 transfection reagent (Mirus Bio) or polyethylenimine reagent (Polysciences Inc.) that was prepared according to manufacturer's protocol.

### **MudPIT proteomic analysis**

MudPIT proteomic analysis was performed as described in [20,34,38] using Finnigan LTQ Linear ion trap mass spectrometer equipped with an electrospray ionization source. T98G cells stably expressing DYRK1A-Flag-HA or GFP-Flag-HA (control) were used for immunoprecipitations with anti-HA antibody agarose beads (clone HA7, Sigma). Proteins were eluted from beads using HA peptide, concentrated and digested with trypsin. Tryptic peptides were resolved using Quaternary Agilent 1100 series HPLC and microcapillary multi-dimensional C<sub>18</sub>-SCX-C<sub>18</sub> matrix using fully automated 10-step chromatography run and electrosprayed into mass spectrometer. Full MS spectra were recorded on the peptides over a 400 to 1,600 m/z range, followed by five tandem mass (MS/MS) events sequentially generated in a data-dependent manner on the first to fifth most intense ions selected from the full MS spectrum (at 35% collision energy). SEQUEST [72] was used to matchMS/MS spectra to peptides in a database of 58622 amino acid sequences, consisting of 29147 Human proteins (non-redundant entries from NCBI 2011-08-16 release). To estimate relative protein levels, spectral counts were normalized using Normalized Spectral Abundance Factors (NSAFs) [34,56,73]. Average NSAFs were calculated from four biological replicate DYRK1A pull-down experiments. Original mass spectrometry data underlying this manuscript can be accessed from the Stowers Original Data Repository at LIBPB-1088.

### **Kinase assays**

For RNF169 phosphorylation assays, HEK293T cells were transfected with HA-tagged RNF169 constructs and lysed using RIPA buffer (50 mM Tris-HCl, pH 7.4, 150 mM NaCl, 1% NP-40, 0.5% Sodium deoxycholate and 0.1% SDS) supplemented with phosphatase and protease inhibitor cocktails (Millipore) and 1:10,000  $\beta$ -mercaptoethanol ( $\beta$ -ME). Extracts were incubated with 1  $\mu$ g anti-HA antibody and protein A beads followed by washes in EBC buffer (50 mM Tris-HCl, pH 8.0,

5 mM EDTA, 120 mM NaCl and 0.5% NP-40), and one final wash with kinase assay buffer (Cell Signaling) containing 25 mM Tris-HCl, pH 7.5, 5 mM  $\beta$ -glycerophosphate, 2 mM DTT, 0.1 mM Na<sub>3</sub>VO<sub>4</sub>, 10 mM MgCl<sub>2</sub>. The immunoprecipitates were used as substrates in a kinase assay reaction in the presence of 1  $\mu$ M cold ATP, 5  $\mu$ Ci of [ $\gamma$ -<sup>32</sup>P] ATP and 200 ng GST-DYRK1A (Life Technologies) for 30 min at RT. The beads containing phosphorylated proteins were washed once with EBC buffer and analyzed by SDS-PAGE and autoradiography. LIN52 phosphorylation assays were performed as described in [74]. Briefly, extracts from control and DYRK1A-KO U-2 OS cell lines (1 mg/ml) were prepared using EDTA-free EBC buffer supplemented with phosphatase inhibitors, 2 mM DTT, 10 mM MgCl<sub>2</sub>, 10 mM MnCl<sub>2</sub> and 200  $\mu$ M ATP, and incubated at 30°C with 6 ng/ $\mu$ l GST-LIN52. Reactions were terminated at different times by adding SDS-PAGE loading buffer and heating at 95°C for 10 min, and analyzed by WB with indicated antibodies as described in [20].

### **Immunofluorescence**

Cells were seeded on glass coverslips in 6-well dishes and allowed to attach for 24h. After washing in PBS three times, cells were fixed in 4% formaldehyde for 20 min and permeabilized with 0.2% Triton X-100 in PBS containing 5% BSA for 30 min followed by incubation with primary and secondary antibodies. The coverslips were mounted in Fluoroshield mounting medium with DAPI (Abcam) and viewed using Zeiss Axio AX10 Imager fluorescence microscope. Images were acquired at 60x magnification using AxioVision software. The images were analyzed using Image J FIJI software [75]. Briefly, images in JPEG format were processed to find the total number of foci (maxima). A noise tolerance value of 20 or 30 was used, and it was the same for all samples within each comparison group. For 53BP1, average foci per cell and number of cells with greater than 10 foci were calculated. For HA-RNF169, average foci per HA-positive cell and number of HA-positive cells with greater than 5 or 10 foci were calculated. To analyze 53BP1 in HA-RNF



169 expressing cell lines, 53BP1 foci were scored only in the HA-positive cells. At least three biological repeats, defined as independently plated and treated series of cell samples, were analyzed for each quantitative analysis. For each biological repeat, more than 100 cells per experimental condition were typically scored. Some experiments were analyzed by two different observers, and all data were included in the analysis.

### **Immunoblotting and immunoprecipitation**

For immunoblotting, cells were lysed in EBC or RIPA buffers for 10 min at 4°C and then centrifuged at 14,000g for 15 min at 4°C. Protein concentrations were determined by DC protein assay (BioRad). Protein samples were resolved using polyacrylamide gels (BioRad), transferred to a nitrocellulose membrane (GE Healthcare) and probed by specific antibodies, as recommended by manufacturer. For immunoprecipitation, cell extracts were incubated with appropriate antibodies (1 µg/ml) and Protein A Sepharose beads (GE Healthcare) overnight at 4°C, washed five times with lysis buffer and resuspended in Laemmli sample buffer (BioRad). Commercially available antibodies used in this study are listed in Supplemental Table 2. Antibodies against LIN52 and phospho-S28-LIN52 (Bethyl) were described in [20]. Rabbit antibodies against DCAF7, FAM117B, LZTS1, LZTS2 and TROAP were also produced by Bethyl.

### **Glycerol gradient centrifugation**

T98G cells were scraped using ice-cold PBS containing protease and phosphatase inhibitors, collected by centrifugation and extracted using buffer containing 10 mM HEPES, 2 mM MgCl<sub>2</sub>, 10 mM KCl, 0.5% NP-40, 0.5 mM EDTA, 150 mM NaCl, H<sub>2</sub>O, 1 mM DTT, protease and phosphatase inhibitors. For glycerol gradient analysis, 200 µL of clarified cell lysate containing approximately 6 mg/ml of protein was loaded on top of a pre-formed glycerol gradient (5 ml, 5–45% in lysis buffer). Another gradient was also loaded with protein weight markers (25 µg each) including bovine serum albumin (Sigma A8531), yeast alcohol

dehydrogenase from yeast (Sigma A 8656), and bovine thyroglobulin (Sigma T9145). The samples were then centrifuged using SW55Ti rotor at 45,000 rpm at 4°C for 18h, after which 200 µL fractions were collected from the top of the gradient and analyzed by Western blotting or Coomassie staining (for markers).

### **DSB repair assay**

DR-GFP reporter cell lines were established by transfecting the DR-GFP reporter construct (gift from Maria Jasin, Addgene plasmid # 26475 [52]) into the control or DYRK1A-KO U-2 OS cells followed by puromycin selection as described in [69]. The cells stably expressing the DR-GFP reporter were infected with adenovirus to express I-SceI at MOI 50. To monitor the HRR efficiency, GFP positive cells were detected 48h post-infection using flow cytometry as described in [52,69].

### **Cell cycle analysis**

U-2 OS WT and DYRK1A-KO CRISPR cells were seeded in 10 cm dishes at a density of  $0.5 \times 10^6$ – $1 \times 10^6$  cells/dish. After 5 Gy or 15 Gy irradiation and incubation for 24h, the cells were harvested and incubated with 0.05 mg/mL propidium iodide in 3.8 mM sodium citrate buffer containing 0.1% Triton X-100 and RNase A solution (Sigma, R4642), and incubated at room temperature for 1h. The cells (at least 10,000 per condition) were then analyzed using FACS Canto II flow cytometer (Becton Dickinson, San Jose, CA, USA).

### **Statistical analysis and bioinformatic tools**

For quantitation of cell-based experiments, 100 or more cells per conditions were typically scored. To calculate statistical significance, data from at least three biological replicates was analyzed using two-tailed Student's t-test. For protein networks analysis, list of proteins detected in at least three out of four DYRK1A MudPIT analyzes was analyzed using MetaScape web-based software (metascape.org) that integrates data from BioGrid [55] and other protein databases with custom datasets to build protein-protein interaction networks.

## Acknowledgments

Authors acknowledge Y. Skversky and S. Gruszecki for technical help, A. Iness for manuscript editing, E. Ivanova and M. Tollenare for help with cell imaging and G. D'Arcangelo for GFP-Dyrk1A constructs. We are grateful to N. Mailand for RNF169 constructs and for helpful suggestions regarding the manuscript. This study was in part supported by the NIH-NCI R01CA188571 (L.L.). Proteomic studies were in part supported by the Stowers Institute for Biomedical Research. Services in support of this research project were generated by the VCU Massey Cancer Center Flow Cytometry Shared Resource as well as the VCU Microscopy Facility supported, in part, with funding from NIH-NCI Cancer Center Support Grant P30 CA016059.

## Disclosure statement

No potential conflict of interest was reported by the authors.

## Funding

This work was supported by the National Institutes of Health [grants R01CA188571, P30 CA016059]; Stowers Institute for Medical Research.

## References

- [1] Birchler JA, Riddle NC, Auger DL, et al. Dosage balance in gene regulation: biological implications. *Trends Genet.* 2005 Apr;21(4):219–226. PubMed PMID: 15797617.
- [2] Veitia RA, Potier MC. Gene dosage imbalances: action, reaction, and models. *Trends Biochem Sci.* 2015 Jun;40(6):309–317. PubMed PMID: 25937627.
- [3] Korb J, Tirosch-Wagner T, Urban AE, et al. The genetic architecture of Down syndrome phenotypes revealed by high-resolution analysis of human segmental trisomies. *Proc Natl Acad Sci U S A.* 2009 Jul 21;106(29):12031–12036. PubMed PMID: 19597142.
- [4] Ohira M, Seki N, Nagase T, et al. Gene identification in 1.6-Mb region of the Down syndrome region on chromosome 21. *Genome Res.* 1997 Jan;7(1):47–58. PubMed PMID: 9037601.
- [5] Ji J, Lee H, Argiropoulos B, et al. DYRK1A haploinsufficiency causes a new recognizable syndrome with microcephaly, intellectual disability, speech impairment, and distinct facies. *Eur J Hum Genet.* 2015 Oct;23(11):1473–1481. PubMed PMID: 25944381; PubMed Central PMCID: PMC4613469.
- [6] Bronicki LM, Redin C, Drunat S, et al. Ten new cases further delineate the syndromic intellectual disability phenotype caused by mutations in DYRK1A. *Eur J Hum Genet.* 2015 Nov;23(11):1482–1487. PubMed PMID: 25920557; PubMed Central PMCID: PMC4613470.
- [7] Guimera J, Casas C, Pucharcos C, et al. A human homologue of *Drosophila* minibrain (MNB) is expressed in the neuronal regions affected in Down syndrome and maps to the critical region. *Hum Mol Genet.* 1996 Sep;5(9):1305–1310. PubMed PMID: 8872470.
- [8] Tejedor F, Zhu XR, Kaltenbach E, et al. minibrain: a new protein kinase family involved in postembryonic neurogenesis in *Drosophila*. *Neuron.* 1995 Feb;14(2):287–301. PubMed PMID: 7857639.
- [9] Tejedor FJ, Hammerle B. MNB/DYRK1A as a multiple regulator of neuronal development. *FEBS J.* 2011 Jan;278(2):223–235. PubMed PMID: 21156027.
- [10] Ahn KJ, Jeong HK, Choi HS, et al. DYRK1A BAC transgenic mice show altered synaptic plasticity with learning and memory defects. *Neurobiol Dis.* 2006 Jun;22(3):463–472. PubMed PMID: 16455265.
- [11] Altafaj X, Dierssen M, Baamonde C, et al. Neurodevelopmental delay, motor abnormalities and cognitive deficits in transgenic mice overexpressing Dyrk1A (minibrain), a murine model of Down's syndrome. *Hum Mol Genet.* 2001 Sep 1;10(18):1915–1923. PubMed PMID: 11555628.
- [12] Raveau M, Shimohata A, Amano K, et al. DYRK1A-haploinsufficiency in mice causes autistic-like features and febrile seizures. *Neurobiol Dis.* 2018 Feb;110:180–191. PubMed PMID: 29223763.
- [13] Fotaki V, Martinez De Lagran M, Estivill X, et al. Haploinsufficiency of Dyrk1A in mice leads to specific alterations in the development and regulation of motor activity. *Behav Neurosci.* 2004 Aug;118(4):815–821. PubMed PMID: 15301607.
- [14] Aranda S, Laguna A, de la Luna S. DYRK family of protein kinases: evolutionary relationships, biochemical properties, and functional roles. *FASEB J.* 2010 Feb;25(2):449–462. PubMed PMID: 21048044.
- [15] Kannan N, Neuwald AF. Evolutionary constraints associated with functional specificity of the CMGC protein kinases MAPK, CDK, GSK, SRPK, DYRK, and CK2alpha. *Protein Sci.* 2004 Aug;13(8):2059–2077. PubMed PMID: 15273306.
- [16] Najas S, Arranz J, Lochhead PA, et al. DYRK1A-mediated cyclin D1 degradation in neural stem cells contributes to the neurogenic cortical defects in down syndrome. *EBioMedicine.* 2015 Feb;2(2):120–134. PubMed PMID: 26137553; PubMed Central PMCID: PMC4484814.
- [17] Di Vona C, Bezdán D, Islam AB, et al. Chromatin-wide profiling of DYRK1A reveals a role as a gene-specific RNA polymerase II CTD kinase. *Mol Cell.* 2015 Feb 5;57(3):506–520. PubMed PMID: 25620562.
- [18] Soppa U, Schumacher J, Florencio Ortiz V, et al. The Down syndrome-related protein kinase DYRK1A phosphorylates p27(Kip1) and Cyclin D1 and induces cell cycle exit and neuronal differentiation. *Cell Cycle.*

- 2014;13(13):2084–2100. PubMed PMID: 24806449; PubMed Central PMCID: PMC4111700.
- [19] Chen JY, Lin JR, Tsai FC, et al. Dosage of Dyrk1a shifts cells within a p21-Cyclin D1 signaling map to control the decision to enter the cell cycle. *Mol Cell*. 2013 Oct 10;52(1):87–100. PubMed PMID: 24119401.
- [20] Litovchick L, Florens L, Swanson SK, et al. DYRK1A protein kinase promotes quiescence and senescence through DREAM complex assembly. *Genes Dev*. 2011;25:801–813. PubMed PMID: 21498570; PubMed Central PMCID: PMC3078706.
- [21] Park J, Song WJ, Chung KC. Function and regulation of Dyrk1A: towards understanding Down syndrome. *Cell Mol Life Sci*. 2009 Oct;66(20):3235–3240. PubMed PMID: 19685005.
- [22] Becker W, Sippl W. Activation, regulation, and inhibition of DYRK1A. *FEBS J*. 2011 Jan;278(2):246–256. PubMed PMID: 21126318.
- [23] Himpel S, Tegge W, Frank R, et al. Specificity determinants of substrate recognition by the protein kinase DYRK1A. *J Biol Chem*. 2000 Jan 28;275(4):2431–2438. PubMed PMID: 10644696.
- [24] Alvarez M, Altafaj X, Aranda S, et al. DYRK1A autophosphorylation on serine residue 520 modulates its kinase activity via 14-3-3 binding. *Mol Biol Cell*. 2007 Apr;18(4):1167–1178. PubMed PMID: 17229891; PubMed Central PMCID: PMC1838983.
- [25] Kim D, Won J, Shin DW, et al. Regulation of Dyrk1A kinase activity by 14-3-3. *Biochem Biophys Res Commun*. 2004 Oct 15;323(2):499–504. PubMed PMID: 15369779.
- [26] Miyata Y, Nishida E. DYRK1A binds to an evolutionarily conserved WD40-repeat protein WDR68 and induces its nuclear translocation. *Biochim Biophys Acta*. 2011 Oct;1813(10):1728–1739. PubMed PMID: 21777625.
- [27] Ritterhoff S, Farah CM, Grabitzki J, et al. The WD40-repeat protein Han11 functions as a scaffold protein to control HIPK2 and MEKK1 kinase functions. *Embo J*. 2010 Nov 17;29(22):3750–3761. PubMed PMID: 20940704.
- [28] Varjosalo M, Keskitalo S, Van Drogen A, et al. The protein interaction landscape of the human CMGC kinase group. *Cell Rep*. 2013 Apr 25;3(4):1306–1320. PubMed PMID: 23602568.
- [29] Subramanian T, Zhao LJ, Chinnadurai G. Interaction of CtBP with adenovirus E1A suppresses immortalization of primary epithelial cells and enhances virus replication during productive infection. *Virology*. 2013 Sep 1;443(2):313–320. PubMed PMID: 23747199; PubMed Central PMCID: PMC3732182.
- [30] Kuppaswamy M, Subramanian T, Kostas-Polston E, et al. Functional similarity between E6 proteins of cutaneous human papillomaviruses and the adenovirus E1A tumor-restraining module. *J Virol*. 2013 Jul;87(13):7781–7786. PubMed PMID: 23637414; PubMed Central PMCID: PMC3700293.
- [31] Cohen MJ, Yousef AF, Massimi P, et al. Dissection of the C-terminal region of E1A redefines the roles of CtBP and other cellular targets in oncogenic transformation. *J Virol*. 2013 Sep;87(18):10348–10355. PubMed PMID: 23864635; PubMed Central PMCID: PMC3753994.
- [32] Komorek J, Kuppaswamy M, Subramanian T, et al. Adenovirus type 5 E1A and E6 proteins of low-risk cutaneous beta-human papillomaviruses suppress cell transformation through interaction with FOXK1/K2 transcription factors. *J Virol*. 2010 Mar;84(6):2719–2731. PubMed PMID: 20053746.
- [33] Guiley KZ, Liban TJ, Felthousen JG, et al. Structural mechanisms of DREAM complex assembly and regulation. *Genes Dev*. 2015 May 1;29(9):961–974. PubMed PMID: 25917549; PubMed Central PMCID: PMC4421984.
- [34] Litovchick L, Sadasivam S, Florens L, et al. Evolutionarily conserved multisubunit RBL2/p130 and E2F4 protein complex represses human cell cycle-dependent genes in quiescence. *Mol Cell*. 2007 May 25;26(4):539–551. PubMed PMID: 17531812.
- [35] Chen J, Feng W, Jiang J, et al. Ring finger protein RNF169 antagonizes the ubiquitin-dependent signaling cascade at sites of DNA damage. *J Biol Chem*. 2012 Aug 10;287(33):27715–27722. PubMed PMID: 22733822.
- [36] Panier S, Ichijima Y, Fradet-Turcotte A, et al. Tandem protein interaction modules organize the ubiquitin-dependent response to DNA double-strand breaks. *Mol Cell*. 2012 Aug 10;47(3):383–395. PubMed PMID: 22742833.
- [37] Poulsen M, Lukas C, Lukas J, et al. Human RNF169 is a negative regulator of the ubiquitin-dependent response to DNA double-strand breaks. *J Cell Biol*. 2012 Apr 16;197(2):189–199. PubMed PMID: 22492721.
- [38] Florens L, Washburn MP. Proteomic analysis by multi-dimensional protein identification technology. *Methods Mol Biol*. 2006;328:159–175. PubMed PMID: 16785648.
- [39] Sardi ME, Cai Y, Jin J, et al. Probabilistic assembly of human protein interaction networks from label-free quantitative proteomics. *Proc Natl Acad Sci U S A*. 2008 Feb 5;105(5):1454–1459. PubMed PMID: 18218781.
- [40] An L, Jiang Y, Ng HH, et al. Dual-utility NLS drives RNF169-dependent DNA damage responses. *Proc Natl Acad Sci U S A*. 2017 Apr 4;114(14):E2872–E2881. PubMed PMID: 28325877; PubMed Central PMCID: PMC5389323.
- [41] Panier S, Boulton SJ. Double-strand break repair: 53BP1 comes into focus. *Nat Rev Mol Cell Biol*. 2014 Jan;15(1):7–18. PubMed PMID: 24326623.
- [42] Tripathi S, Pohl MO, Zhou Y, et al. Meta- and orthogonal integration of influenza “OMICs” data defines a role for UBR4 in virus budding. *Cell Host Microbe*. 2015 Dec 09;18(6):723–735. PubMed PMID: 26651948; PubMed Central PMCID: PMC4829074.

- [43] Subramanian A, Tamayo P, Mootha VK, et al. Gene set enrichment analysis: a knowledge-based approach for interpreting genome-wide expression profiles. *Proc Natl Acad Sci U S A*. 2005 Oct 25;102(43):15545–15550. PubMed PMID: 16199517; PubMed Central PMCID: PMC1239896.
- [44] Himpel S, Panzer P, Eirnbter K, et al. Identification of the autophosphorylation sites and characterization of their effects in the protein kinase DYRK1A. *Biochem J*. 2001 Nov 1;359(Pt 3):497–505. PubMed PMID: 11672423.
- [45] Schneider CA, Rasband WS, Eliceiri KW. NIH image to ImageJ: 25 years of image analysis. *Nat Methods*. 2012 Jul;9(7):671–675. PubMed PMID: 22930834; PubMed Central PMCID: PMC5554542.
- [46] Hornbeck PV, Kornhauser JM, Tkachev S, et al. PhosphoSitePlus: a comprehensive resource for investigating the structure and function of experimentally determined post-translational modifications in man and mouse. *Nucleic Acids Res*. 2012 Jan;40(Database issue):D261–D270. PubMed PMID: 22135298; PubMed Central PMCID: PMC3245126.
- [47] Hu Q, Botuyan MV, Cui G, et al. Mechanisms of ubiquitin-nucleosome recognition and regulation of 53BP1 chromatin recruitment by RNF168/169 and RAD18. *Mol Cell*. 2017 May 18;66(4):473–487 e9. PubMed PMID: 28506460; PubMed Central PMCID: PMC5523955.
- [48] Cong L, Ran FA, Cox D, et al. Multiplex genome engineering using CRISPR/Cas systems. *Science*. 2013 Feb 15;339(6121):819–823. PubMed PMID: 23287718; PubMed Central PMCID: PMC3795411.
- [49] Barretina J, Caponigro G, Stransky N, et al. The cancer cell line encyclopedia enables predictive modelling of anticancer drug sensitivity. *Nature*. 2012 Mar 29;483(7391):603–607. PubMed PMID: 22460905; PubMed Central PMCID: PMC3320027.
- [50] Canny MD, Moatti N, Wan LCK, et al. Inhibition of 53BP1 favors homology-dependent DNA repair and increases CRISPR-Cas9 genome-editing efficiency. *Nat Biotechnol*. 2018 Jan;36(1):95–102. PubMed PMID: 29176614; PubMed Central PMCID: PMC5762392.
- [51] Durocher D, Pelletier L. 53BP1 goes back to its p53 roots. *Mol Cell*. 2016 Oct 6;64(1):3–4. PubMed PMID: 27716486.
- [52] Pierce AJ, Johnson RD, Thompson LH, et al. XRCC3 promotes homology-directed repair of DNA damage in mammalian cells. *Genes Dev*. 1999 Oct 15;13(20):2633–2638. PubMed PMID: 10541549; PubMed Central PMCID: PMC317094.
- [53] Dierssen M, de Lagran MM. DYRK1A (dual-specificity tyrosine-phosphorylated and -regulated kinase 1A): a gene with dosage effect during development and neurogenesis. *ScientificWorldJournal*. 2006;6:1911–1922. PubMed PMID: 17205196.
- [54] Abbassi R, Johns TG, Kassiou M, et al. DYRK1A in neurodegeneration and cancer: molecular basis and clinical implications. *Pharmacol Ther*. 2015 Jul;151:87–98. PubMed PMID: 25795597.
- [55] Chatr-Aryamontri A, Breitkreutz BJ, Oughtred R, et al. The BioGRID interaction database: 2015 update. *Nucleic Acids Res*. 2015 Jan;43(Database issue):D470–D478. PubMed PMID: 25428363; PubMed Central PMCID: PMC4383984.
- [56] Swanson SK, Florens L, Washburn MP. Generation and analysis of multidimensional protein identification technology datasets. *Methods Mol Biol*. 2009;492:1–20. PubMed PMID: 19241024.
- [57] Glenewinkel F, Cohen MJ, King CR, et al. The adaptor protein DCAF7 mediates the interaction of the adenovirus E1A oncoprotein with the protein kinases DYRK1A and HIPK2. *Sci Rep*. 2016 Jun 16;6:28241. PubMed PMID: 27307198; PubMed Central PMCID: PMC4910162.
- [58] Peng Z, Liao Z, Matsumoto Y, et al. Human DNA ligase I interacts with and is targeted for degradation by the DCAF7 specificity factor of the Cul4-DDB1 ubiquitin ligase complex. *J Biol Chem*. 2016 Oct 14;291(42):21893–21902. PubMed PMID: 27573245; PubMed Central PMCID: PMC5063974.
- [59] Hustedt N, Durocher D. The control of DNA repair by the cell cycle. *Nat Cell Biol*. 2016 Dec 23;19(1):1–9. PubMed PMID: 28008184.
- [60] Doil C, Mailand N, Bekker-Jensen S, et al. RNF168 binds and amplifies ubiquitin conjugates on damaged chromosomes to allow accumulation of repair proteins. *Cell*. 2009 Feb 6;136(3):435–446. PubMed PMID: 19203579.
- [61] Fradet-Turcotte A, Canny MD, Escribano-Diaz C, et al. 53BP1 is a reader of the DNA-damage-induced H2A Lys 15 ubiquitin mark. *Nature*. 2013 Jul 4;499(7456):50–54. PubMed PMID: 23760478; PubMed Central PMCID: PMC3955401.
- [62] Panier S, Durocher D. Regulatory ubiquitylation in response to DNA double-strand breaks. *DNA Repair (Amst)*. 2009 Apr 5;8(4):436–443. PubMed PMID: 19230794.
- [63] Escribano-Diaz C, Orthwein A, Fradet-Turcotte A, et al. A cell cycle-dependent regulatory circuit composed of 53BP1-RIF1 and BRCA1-CtIP controls DNA repair pathway choice. *Mol Cell*. 2013 Mar 7;49(5):872–883. PubMed PMID: 23333306.
- [64] Isono M, Niimi A, Oike T, et al. BRCA1 directs the repair pathway to homologous recombination by promoting 53BP1 dephosphorylation. *Cell Rep*. 2017 Jan 10;18(2):520–532. PubMed PMID: 28076794.
- [65] Liu X, Yang X, Li Y, et al. Trip12 is an E3 ubiquitin ligase for USP7/HAUSP involved in the DNA damage response. *FEBS Lett*. 2016 Dec;590(23):4213–4222. PubMed PMID: 27800609.
- [66] Yim H, Shin SB, Woo SU, et al. Plk1-mediated stabilization of 53BP1 through USP7 regulates centrosome



- positioning to maintain bipolarity. *Oncogene*. 2017 Feb 16;36(7):966–978. PubMed PMID: 27477698.
- [67] Zhu Q, Sharma N, He J, et al. USP7 deubiquitinase promotes ubiquitin-dependent DNA damage signaling by stabilizing RNF168. *Cell Cycle*. 2015;14(9):1413–1425. PubMed PMID: 25894431; PubMed Central PMCID: PMC4613370.
- [68] Chapman JR, Sossick AJ, Boulton SJ, et al. BRCA1-associated exclusion of 53BP1 from DNA damage sites underlies temporal control of DNA repair. *J Cell Sci*. 2012 Aug 1;125(Pt 15):3529–3534. PubMed PMID: 22553214; PubMed Central PMCID: PMC3445322.
- [69] Yakovlev VA. Nitric oxide-dependent downregulation of BRCA1 expression promotes genetic instability. *Cancer Res*. 2013 Jan 15;73(2):706–715. PubMed PMID: 23108140; PubMed Central PMCID: PMC3549017.
- [70] Jaspers JE, Kersbergen A, Boon U, et al. Loss of 53BP1 causes PARP inhibitor resistance in Brca1-mutated mouse mammary tumors. *Cancer Discov*. 2013 Jan;3(1):68–81. PubMed PMID: 23103855.
- [71] Yabut O, Domogauer J, D’Arcangelo G. Dyrk1A overexpression inhibits proliferation and induces premature neuronal differentiation of neural progenitor cells. *J Neurosci*. 2010 Mar 17;30(11):4004–4014. PubMed PMID: 20237271.
- [72] Eng J, McCormack AL, Yates JR III. An approach to correlate tandem mass spectral data of peptides with amino acid sequences in a protein database. *J Am Mass Spectrom*. 1994;5:976–989.
- [73] Zybaylov B, Mosley AL, Sardu ME, et al. Statistical analysis of membrane proteome expression changes in *Saccharomyces cerevisiae*. *J Proteome Res*. 2006 Sep;5(9):2339–2347. PubMed PMID: 16944946.
- [74] Iness AN, Felthousen J, Ananthapadmanabhan V, et al. The cell cycle regulatory DREAM complex is disrupted by high expression of oncogenic B-Myb. *Oncogene*. 2018 Sep 11. PubMed PMID: 30206359.
- [75] Schindelin J, Arganda-Carreras I, Frise E, et al. Fiji: an open-source platform for biological-image analysis. *Nat Methods*. 2012 Jun 28;9(7):676–682. PubMed PMID: 22743772; PubMed Central PMCID: PMC3855844.